Hot-Electron Injection in Au Nanorod-ZnO Nanowire Hybrid Device for Near-Infrared Photodetection

Andrea Pescaglini,[†] *Alfonso Martín,*[†] *Davide Cammi ,*[‡] *Gediminas Juska,*[†] *Carsten Ronning*[‡] *Emanuele Pelucchi*[†] *and Daniela Iacopino*[†]*

[†] Tyndall National Institute – University College Cork, Lee Maltings, Cork, Ireland

[‡] Institute of Solid State Physics, Friedrich Schiller University of Jena, Max-Wien-Platz 1, 07743 Jena, Germany

*Corresponding author: daniela.iacopino@tyndall.ie

KEYWORDS: Plasmon, hot electron, nanowire, Au nanorod, photodetector

In this paper we present a new class of near-infrared photodetectors comprising Au nanorods – ZnO nanowire hybrid systems. Fabricated hybrid FET devices showed a large photoresponse under radiation wavelengths between 650 nm and 850 nm, accompanied by an “ultrafast” transient with a time scale of 250 ms, more than one order of magnitude faster than the ZnO response under radiation above band-gap. The generated photocurrent is ascribed to plasmonic-mediated generation of hot electrons at the metal-semiconductor Schottky barrier. In the

presented architecture Au nanorod localized surface plasmons were used as active elements for generating and injecting hot-electrons into the wide band-gap ZnO nanowire, functioning as a passive component for charge collection. A detailed investigation of the hot-electron generation and injection processes is discussed to explain the improved and extended performance of the hybrid device. The quantum efficiency measured at 650 nm was calculated to be approximately 3%, more than 30 times larger than values reported for equivalent metal/semiconductor planar photodetectors. The presented work is extremely promising for further development of novel miniaturized, tunable photodetectors and for highly efficient plasmonic energy conversion devices.

Plasmonic nanostructures have been extensively studied for their unique ability to focus light into nanometer-scale volumes due to large localized electromagnetic fields generated by surface plasmons.[1] Recently, potential applications have been widened by the observation that plasmonic nanostructures can also directly convert the collected light into electrical energy by generation of so called “hot electrons”, whereby surface plasmons excited by incident radiation can decay non-radiatively and generate an energetic electron instead of re-emitting a photon.[2] Such generated hot electrons usually relax to the ground state through electron-electron and electron-phonon interactions. However, when a hot electron with sufficient momentum is generated in a metallic nanostructure in direct contact with a semiconductor where an interface potential is formed (Schottky barrier like in the broad sense), the excited electron in the nanostructures might have sufficient energy to traverse the barrier. This effect can result in generation of enhanced photocurrent while exciting at photon energies below the band-gap of the semiconductor and

confers widened optoelectronic features to the resulting metal-semiconductor hybrid device. The first evidence of hot electron generation and injection was reported by Zhao *et al.*[3], who investigated the photoelectrochemical response of TiO_2 film electrodes containing Au and Ag nanoparticles. They observed an anodic photocurrent peak at 560 nm, which they attributed to the surface plasmon resonance of metal nanoparticles. More recently, Tian *et al.* demonstrated a maximum incident photon to current conversion efficiency (IPCE) of almost 6% in Au nanoparticle sensitized solid-state heterojunction solar cells containing optimized redox couples to regenerate charge in the metal nanoparticles within 20 ns after injection.[4] Enhanced photocatalytic activity mediated by surface plasmons was also demonstrated in TiO_2 nanotubes and nanospheres.[5, 6]

The first example of hot electron generation for photodetection applications has been proposed by Knight *et al.* who fabricated Au resonant antennas on a n-type silicon substrate electrically connected through a top transparent electrode of indium tin oxide (ITO). The device generated photocurrent under radiation wavelengths 1250-1600 nm, displaying a maximum value in correspondence of the plasmonic resonance of the optical antenna.[7] The initial quantum efficiency of 0.01% was subsequently increased by about one order of magnitude by embedding the plasmonic structure within the semiconductor, thus creating a 3D Schottky barrier.[8]

Overall, the field of plasmonic hot-electron generation in nanostructures is still at its infancy. Therefore, alternative plasmonic/semiconductor material combinations together with alternative device geometries could be explored, potentially leading to generation of detectors with higher efficiencies and extended tunable wavelength ranges. For example, Fang *et al.* fabricated nanoscale antennas sandwiched between two graphene monolayers that efficiently converted visible and near-infrared photons into electrons with an 800% enhancement of the photocurrent

relative to the antennaless device.[9] Furthermore, the transition from 3D architectures to 1D architectures based on semiconductor nanowires has been shown to support faster carrier collection[10] and to allow use of a wider range of semiconductor materials.[11] Plasmonic-enhanced photocurrent and optical absorption were observed in Si nanowires, induced by the enhanced electric field at the metal/semiconductor interface.[12-14] Enhanced optical absorption was also observed in hybrid InAs nanowires[15] and GaAs nanowires.[16]

Among semiconductor nanowires, ZnO nanostructures have been extensively investigated for optoelectronic applications due to their large band-gap energy (3.3 eV) and ease and low cost of manufacturing.[17-20] Several authors have investigated metal nanostructure-ZnO nanowire hybrid systems. For example band-edge emission photoluminescence and photocurrent enhancement, originating from metal to ZnO electron transfer, were detected in ZnO nanowires coated with metal nanoparticles.[21-23] However, plasmonic-mediated generation, injection and collection of energetic electrons in semiconductor nanowire-based hybrid devices for photodetection and photovoltaic applications remain a field vastly unexplored.

In this article, we present intense near infrared photon-generated hot electrons in individual ZnO nanowire FETs (Field Effect Transistor) decorated with Au nanorods. The hybrid system displayed large photocurrents under irradiation between 650 nm and 850 nm, accompanied by an "ultrafast" response (for the system) with a time scale of 250 ms, more than one order of magnitude faster than the response of bare ZnO nanowires above band-gap radiation. Photoresponse arose by efficient hot-electrons generation and injection at the metal-semiconductor interface. Thus, in the proposed hybrid system Au nanorods acted as active elements, generating hot electrons that were injected into the wide band-gap ZnO nanowire, which functioned as a passive component for charge collection. A detailed investigation of the

effect played by the Au nanorods on the process showed that the density of nanorods deposited on the nanowire affected photocurrent intensities and the height of the Schottky barrier. Theoretical predictions and simulations supported the experimental findings and showed that the selected nanorod anisotropic shape and size played a pivotal role in the hot-electron generation and injection processes. To the best of our knowledge this is the first report on hot-electron injection mediated by localized surface plasmons in hybrid metal nanorod-semiconductor nanowire FET devices.

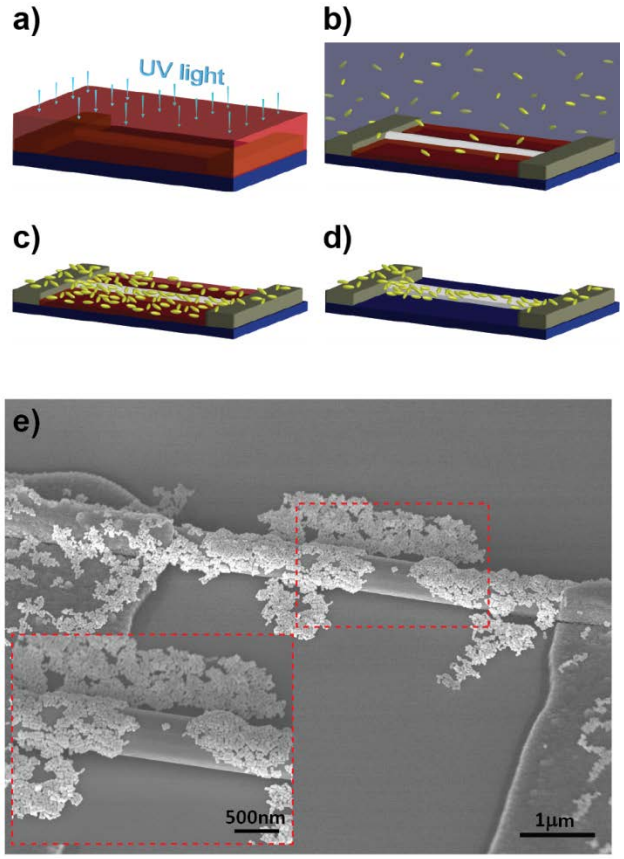

Figure 1. Schematic description of nanorod deposition process. a) Deposition of esist layer on ZnO nanowire FET by spin-coating ; b) deposition of colloidal Au nanorod solution droplet on the substrate; c) nanorod deposited on the substrate following solvent evaporation; d) resist lift-off leaving nanorod deposited on ZnO nanowire and electrodes; e) SEM image of a

representative hybrid device. Inset: close-up SEM image of Au nanorod deposited on the ZnO nanowire.

ZnO nanowire FET devices were fabricated by deposition of ZnO nanowires on clean $Si(n^{++})/SiO_2$ (300 nm) surfaces, followed by electrical contacting by standard optical lithography (metal contacts of Ti/Al 10 nm/200 nm separated by 5 μm gap). Hybrid devices were obtained by selective deposition of colloidal Au nanorods on fabricated ZnO nanowire FET devices. The method is schematically described in Figure 1a-d. Specifically, a resist (S1813, 1.4 μm) layer was deposited on substrates containing ZnO nanowire FETs by spin-coating. The resist was selectively etched by exposition to UV light followed by resist development so that complete removal was achieved on the metal pads and the nanowire top surface, while leaving a residual layer along the nanowire side and on the substrate surface (Figure 1a). Au nanorods were deposited on the entire substrate surface by deposition of aqueous suspensions followed by evaporation at 110 °C (Figure 1b-c). Finally, the residual resist layer was removed leaving Au nanorods selectively deposited on the ZnO surface (Figure 1d). A representative SEM image of the ZnO nanowire FET device decorated with Au nanorods is shown in Figure 1e. A reproducible formation of hybrid devices with randomly oriented nanorods was achieved with the proposed method. Removal of resist in two different phases of the process allowed selective decoration of the ZnO nanowire surface while preventing Au nanorod deposition in the area between contacting electrodes. This avoided the generation of electrical shorts arising from formation of nanorod networks in the area between the electrode gaps.

The photoconductive behavior of hybrid Au nanorods - ZnO nanowire FET devices was investigated under incident radiation at wavelengths between 650 nm and 850 nm (corresponding to a photon energy interval 1.9 - 1.45 eV) and intensity of ~20 W/cm^2 (see SI for further details).

Figure 2a shows measured photocurrent spectra of a hybrid device illuminated at 650 nm and 850 nm. In both cases the dark current was negligible and the curves displayed a sharp increase in intensity concomitant with the onset of illumination. Maximum photoconductivity values of 0.6 nA and 0.26 nA were detected after 15 s of illumination at 650 nm and 850 nm, respectively.

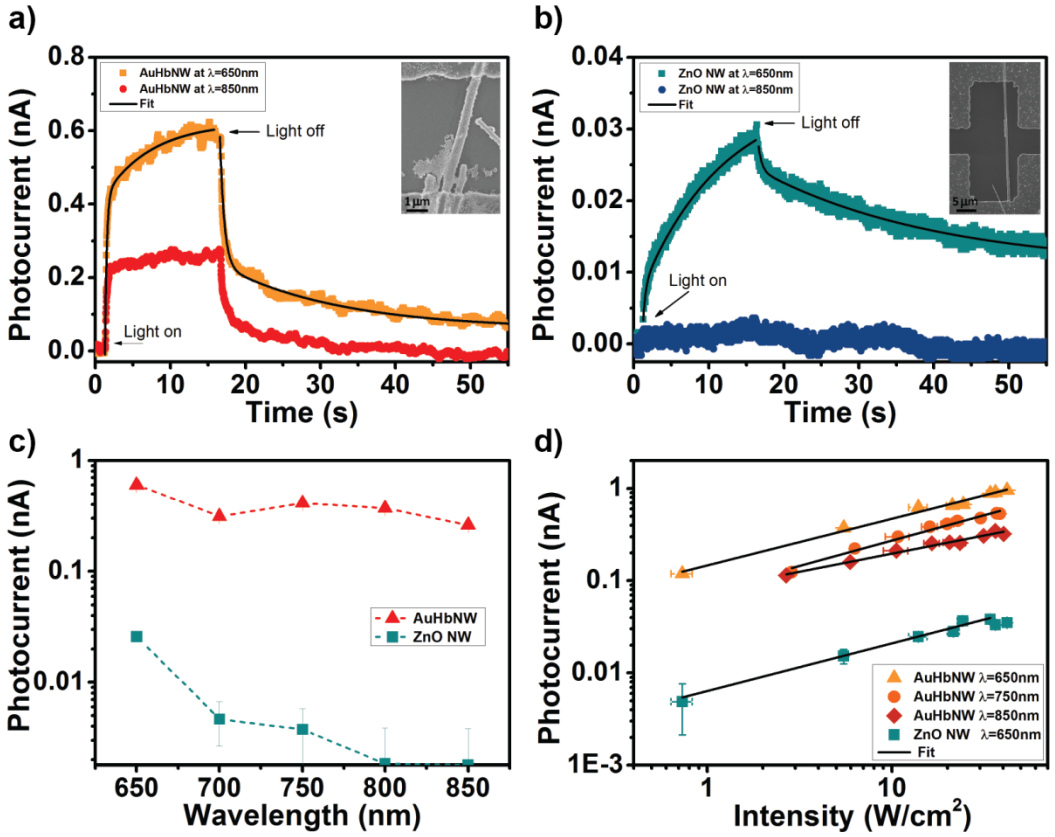

Figure 2. Photoresponse during exposition to light with λ = 650 nm and λ = 850 nm of a) hybrid FET device and b) ZnO nanowire FET. Black lines are the bi-exponential growth and decay fitting to the corresponding data. Insets are the SEM image of the measured devices. c) Photocurrent measured in hybrid and ZnO NW FET device for wavelengths in the range 650-850 nm. d) Power dependence of photocurrent in hybrid and ZnO NW FET devices. Black lines are the linear fits.

Notably the curves showed an equally sharp decrease after interruption of illumination, with only 30% of initial photocurrent measured after 400 ms. In comparison (Figure 2b), bare ZnO FET devices showed a weak photocurrent response, which reached a maximum value of 29 pA after 15 s of illumination at 650 nm. The photo-current decreased by 60% within 55 s of turning off illumination and the dark current value was completely restored only after several minutes. It should be noted that the generation of photocurrent response at excitation energy below the ZnO band gap (3.3 eV) has been already reported in literature [24] and was attributed to the presence of structural defects such as antisite oxide O_{Zn}, Zn vacancy V_{Zn} and oxygen vacancy, V_O.[25] Sub-bandgap photocurrent due to surface state excitation had a maximum in correspondence of the green-yellow photoluminescence band at 2.48 eV [26] (500 nm) and a negligible contribution at lower energies. This is consistent with our findings, reporting no photocurrent generation in ZnO nanowire FET devices under irradiation at 850 nm (compare with Figure 2b).

To further characterize the photocurrent behavior, we investigated photo-generation and photo-decay time scales using a bi-exponential fit of the photocurrent growth and decay defined respectively by [27]

$$I_{ph} = A_0 + A_1 \cdot \left(1 - e^{-\frac{t}{\tau_1}}\right) - A_2 \cdot e^{-\frac{t}{\tau_2}} \quad (1)$$

and

$$I_{ph} = B_0 + B_1 \cdot e^{-\frac{t}{\gamma_1}} + B_2 \cdot e^{-\frac{t}{\gamma_2}} \quad , \quad (2)$$

where A_0, A_1, A_2, τ_1, τ_2 and B_0, B_1, B_2, γ_1, γ_2 were free fit parameters (black lines in Figures 2a-b).

In the hybrid device under excitation at 650 nm two components were calculated for the photocurrent rise and decay, with time constants τ_1 = 6.3±0.4 s and τ_2 = 0.238±0.07 s and γ_1 = 16.5±0.3 s and γ_2 = 0.69±0.01 s, respectively. The relative importance of these two distinctive

processes is given by the coefficients A_1, A_2 and B_1, B_2. The coefficients A_1 = 0.61±0.01 nA, B_1= 0.637±0.002 nA are orders of magnitude smaller than A_2=247±43 nA and B_2= 10±2 μA, indicating that the fast process dominated the photoresponse of hybrid devices.

For bare ZnO nanowire FET devices a slow component rising with time constant τ_1= 10.9±0.4 s and a fast component with time constant τ_2=0.33±0.05 s were calculated. Coefficients A_2, B_2 (8.7 ± 0.6 and 7.8 ± 0.7 pA, respectively) were one order of magnitude smaller than A_1, B_1 (67±1 pA and 33.9 ± 0.2 pA, respectively) indicating that the slow process controlled the photoresponse. Therefore, the overall weight-average time response in hybrid devices τ_{hyb}=0.25 s was almost 40 times faster than ZnO nanowire FET devices (τ_{ZnO}=9.7 s).

Interestingly, although a larger photocurrent was observed under UV irradiation, both ZnO nanowire and hybrid FET devices showed a photoresponse dominated by the slow process (A_1>A_2) (see Figure S2-S3). For photon energy above band-gap, direct generation of electron-hole pairs in ZnO nanowire on sub-nanoseconds time scale is expected to be the main process contributing to the photocarrier generation.[28] However, the longer response time observed indicated a UV photoresponse dominated by electron-hole generation and recombination mediated by deep defects levels.[29] Measurements performed under UV illumination on ZnO nanowire FETs in high vacuum (see Figure S4) showed a considerable increment in the time constants related to photocurrent rise and decay processes compared to air, thus supporting a photocarrier generation involving desorption/re-adsorption of oxygen species in surface trap states.[27, 30]

Photocurrent values measured at different wavelengths between 650 nm and 850 nm for hybrid devices and bare ZnO FET devices are shown in Figure 2c. As the radiation wavelength increased the response of the hybrid device decreased slightly (by a factor of 2). Therefore

measurable values were still achieved at 850 nm, suggesting that further longer wavelengths could be detected in such devices. In contrast, bare ZnO nanowire FETs showed photocurrent values 2 orders of magnitude lower than those measured for hybrid devices. The response was characterized by a marked decrease of photocurrent for wavelengths longer than 650 nm, with no detectable values recorded above 750 nm.

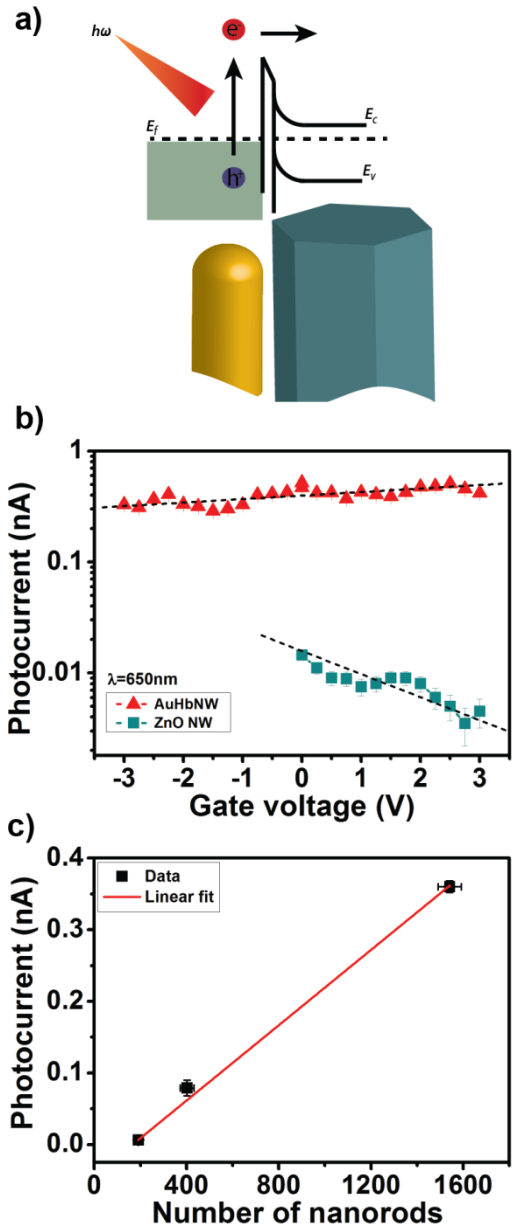

Figure 3. a) Schematic representation of the hot-electron generation and injection processes at the nanorod-nanowire interface. b) Modulation of the photocurrent in bare ZnO nanowire and hybrid FET devices with the applied gate voltage. Dotted lines are guides for the eyes. c) Photocurrent intensity as a function of the number of nanorods in the hybrid device. Red line represents the linear fit to the data.

We also assessed the power dependence of the photoresponse under radiation at 650 nm (Figure 2d). We observed that at low illumination power of 0.6 W/cm^2 the photoresponse of the hybrid device was 0.12 nA, two orders of magnitude larger than the barely detectable photocurrent of ZnO nanowire FETs. This extends the estimated detection limit in the range of mW/cm^2. No evidence of saturation was found in hybrid devices within the explored laser intensity ranges whereas ZnO nanowire FETs displayed saturation above 20 W/cm^2. We also found a sub-linear dependence of photocurrent *vs* power following the power law $I_{ph} \sim P^{\alpha}$ with α=0.51 ±0.08 and 0.50±0.02 for ZnO nanowire FETs and hybrid FETs respectively. In hybrid FETs the α value remained smaller than unity even at longer wavelengths with α=0.55±0.03 at λ=750 nm and α=0.39±0.02 at λ=850 nm. The comparable α values found in the measured devices suggest to attribute the observed behavior to the ZnO nanowire. Sub-linear dependence was previously reported in nanowires of different materials, including Si,[31] ZnO,[10] GaN [32] and ascribed to the saturation of hole-traps and consequent increasing of free electron-hole recombination.[8, 25]

Overall, the fast and enhanced response of hybrid devices under near-infrared radiation could not be associated to the photocarrier dynamics in bare ZnO nanowire FETs. We attributed the photoconductivity behavior observed in hybrid devices to plasmonic-mediated hot electron

generation and injection at the Au nanorod-ZnO nanowire interface. Figure 3a depicts schematically the process. Incident radiation excites localized surface plasmons in Au nanorods. After excitation, localized surface plasmons can decay non-radiatively by transferring energy to electrons, thus creating a distribution of "hot electrons" well above the Fermi energy of the metal. Electrons with energies above the Schottky barrier at the metal-semiconductor interface are directly injected in the conduction band of the ZnO nanowire; electrons with lower energies have an exponentially decreased probability to be injected. The hot-electron generation and injection processes is estimated to take place on the order of sub-picoseconds[33] thus contributing to enhance the fast component of photocurrent growth, in agreement with the experimental observations. It should be noticed that although the presence of an organic ligand shell of ~2 nm on the Au nanorods (see SI) and the Van der Waals bonds (or chemisorption chemical bonds) formed at the ZnO surface do not form a conventional Au-ZnO Schottky contact, the plasmonic-mediated hot-electron injection process previously described is still allowed to occur, in what is by all means an interface (admittedly complex) chemically bonded assembly. The excited hot-electrons in the Au nanorod have a probability to be excited either above whatever barrier is formed or tunnel through it, as previously reported in a number of other ligand-stabilized nanoparticle assembly systems,[34-38] therefore not affecting the mechanism proposed but only the efficiency of the injection rate. When hot-electrons pass the Au nanorod-ZnO nanowire interface, the nanorod remains positively charged. At higher light intensities an increasing number of hot electrons are generated but the restoring electric field built up at the interface limits the injection rate resulting in a sublinear photocurrent increment with the illumination power. Following laser turn off, the fast decrease in conductance is associated to the capture of excess electrons in ZnO conduction band by Au nanorods to restore equilibrium conditions. We

investigated the photocurrent generation process at different back-gate voltages (radiation with energy 1.9 eV and intensity 20 W/cm^2, Figure 3b) for both hybrid devices and ZnO nanowire FETs in order to corroborate the proposed model. Due to the n-type nature of ZnO nanowires (see SI), the application of positive back-gate voltages results in an increase of the nanowire electron density and, in turn, in a reduction of the depletion region near the nanowire surface. Accordingly, ZnO nanowire FETs showed a progressive decrease of the photocurrent for positive applied voltages. This behavior supported the hypothesis that sub-band gap photocurrent is originated from surface defect states localized within the depletion region created by negative oxygen ions adsorbed,[39] Zn vacancies[24] and oxygen vacancies.[26, 29] The photocurrent measured at different back-gate voltages in the hybrid device displayed a clearly distinct behavior, as shown in Figure 3b. A slight increase of the photocurrent was observed with negative to positive applied voltages, showing a weak dependence of the photocurrent from applied back-gate values. However, since the observed trend resembled the transfer characteristic of the ZnO nanowire FETs (see Figure S1b) the variation in photocurrent was ascribed to the changes in the nanowire electron density due to electrostatic effects.

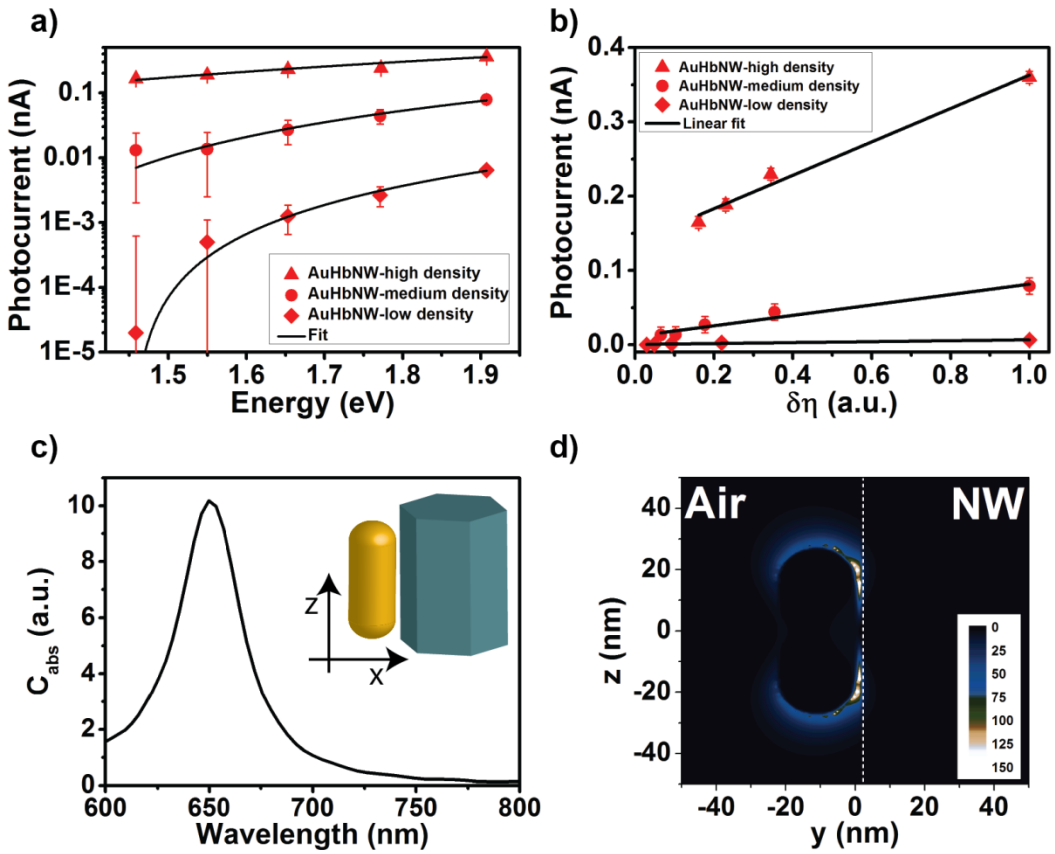

Figure 4. a) Photocurrent dependence from the radiation intensity in hybrid FET devices with increasing number of nanorods. Black line represents the fit using Eq.(3). b) Photocurrent intensity *vs* hot-electron density calculated from Eq.(4) and the relative linear fit (black line). FDTD simulation showing c) absorption cross section and d) the enhanced electric field factor of at Au nanorod-ZnO nanowire interface with 2 nm separation with light polarized along the z direction and incident along x.

The dependence of the hot-electron injection process in relation to the density of deposited nanorods and radiation energy was also investigated. Figure 3c reports the measured photocurrent at 650 nm in three hybrid devices with increasing number of Au nanorods deposited on the surface. The number of Au nanorods were estimated to be 191±20 (low density), 402±30

(medium density) and 1541±50 (high density), calculated by measuring the nanowire area covered by particles divided by the geometrical cross section of a nanorod. A linear increase of the photocurrent was calculated for the three hybrid devices with increasing nanorod densities, thus supporting the plasmonic origin of the measured photocurrent.

Furthermore, Figure 4a shows measured the photocurrent at different radiation energies for hybrid devices with low, medium and high nanorod densities. In a perfect metal-semiconductor junction, the electron injection rate can be well approximated by the Fowler equation[40]

$$I_{ph} \propto (\hbar\omega - \Phi_b)^2 \quad , \qquad (3)$$

where ω is the frequency of the incident radiation and Φ_b the barrier height at the interface. Displayed data in Figure 4a were well fitted with Eq.(3) and gave barrier heights of 1.45±0.03, 1.26±0.05, and 0.56±0.05 eV for low, medium and high density of particles, respectively. In a bare ZnO nanowire, the surface band bending was estimated to be between 1-1.7 eV above the Fermi energy depending on the surface passivation.[41] Φ_b values between 1-1.7 eV were also calculated for low and medium nanorod density hybrid devices, indicating that the barrier at the interface was mainly determined by the properties of the ZnO surface. However, in high particle density hybrid structures, where the nanowire surface was almost completely covered by nanorods, the Φ_b value (0.56 eV) was found to be close to the expected barrier height at the Au-ZnO interface (0.65 eV).[42] Therefore, we deduced that at low nanorod densities the nanorod-semiconductor interface maintained the original properties of the semiconductor surface while for the limiting case of a nanowire fully covered by nanorods the nanorod-semiconductor interface was determined by the difference in work function between materials involved. The value of the interface energy barrier Φ_b plays a fundamental role in determining the rate of hot-

electrons injection. These results provide important indications for optimizing the device by reducing the junction barrier Φ_b.

Finally, we considered the role of nanorod-shaped particles in hot-carriers generation. Govorov *et al.*[42-44] calculated the density of hot-carriers in metal nanocrystals using quantum linear response theory. Efficient relaxation of surface plasmons into one-electron excitations appeared only in metal nanocrystals with dimensions around 20 nm or below, due to the non-conservation of the momentum of electrons in confined systems. Due to the small size of the nanorod used in this work (22x54 nm) we can compare the theoretical prediction with the experimental results. The theoretical hot-carrier density was found dependent from the radiation energy $\nabla\omega$ as follows

$$\delta\eta \propto \frac{|\beta(\omega)|^2}{\omega^4} \quad (4)$$

With $\beta(\omega)$ the field-enhancement factor inside the metal nanostructure that for an ellipsoidal nanorod can be approximated as[45]

$$\beta(\omega) \approx \frac{\varepsilon_m}{3(\varepsilon_m+(\varepsilon_{Au}(\omega)-\varepsilon_m)L_a)} \quad (5)$$

with ε_m and ε_{Au} the dielectric constant of surrounding medium and gold respectively and L_a the depolarizing factor along the main axis of the nanorod (see SI for more details).

Photocurrent values measured in three devices at different radiation energies are plotted versus the hot-electron population $\delta\eta$ calculated from Eq.(4) in Figure 4b. The average geometrical depolarizing factor L_{am} obtained from the statistical length and diameter of the nanorods was 0.13±0.03 (see Eq.(s1)). A linear fitting function was applied by using ε_m=1 and L_a as the only free parameter for the three cases, in excellent agreement with the theory. The extracted values for L_a were 0.095±0.005, 0.118±0.008 and 0.28±0.03 for the devices (i), (ii) and (iii), respectively and perfectly reflected the calculated L_{am} within the error. The increasing of L_a with the nanorod density was attributed to the plasmonic near-field coupling between nanorods. It is

well known that plasmonic resonances of isolated nanoparticles are strongly modified in closely spaced arrays.[46] In particular, for large arrays a blue shift of the main resonance is observed and new resonances at longer wavelength appear. The blue shift corresponds to a change in the aspect ratio of the effective scattering unit towards a more isotropic shape, thus leading to an increasing of the L_a value.

Figure 4c shows the calculated absorption cross section for a nanorod with a dimension of 22x54 nm in close proximity to a ZnO nanowire (separation of 2 nm) by finite-difference time domain (FDTD) simulations using Lumerical Solution software. A plasmonic resonance related to the nanorod longitudinal surface mode was found peaked around 650 nm. The number of hot carriers generated (i.e. the photocurrent) is expected to follow the absorption profile of the nanoparticle,[47] thus reaching the maximum in proximity of the longitudinal surface plasmon and decrease at longer wavelengths. This is in agreement with the experimental results obtained from hybrid devices. We should notice that the cross section of closely spaced nanorods can deviate from the curve showed in Figure 4c due to inter-particle coupling. In particular, a broadening of the resonance peak might occur, so that a contribution at larger wavelengths are expected. Furthermore, FDTD simulations of the electric field enhancement occurring at the interface between closely spaced parallel Au nanorod–ZnO nanowire showed formation of an intense enhanced electromagnetic field in the area between adjacent structures (Figure 4d). It has been shown that only electrons with large enough momentum perpendicular to the metal-semiconductor interface can be efficiently injected into the semiconductor.[40] This constitutes an important limitation to the carrier injection when an electromagnetic radiation propagating perpendicular to the metal-semiconductor junction is used.[8] However, the localized enhanced

field at the interface generated by plasmons in nanorods allows overcoming this limitation and facilitates electron injection inside the semiconductor.

The quantum efficiency of the hybrid device, defined as the number of electrons collected per unit time divided by the number of absorbed photons was calculated to be ~3% at 650 nm, more than 30 times larger than the quantum efficiency reported for planar photodetectors based on hot-electron injection mechanism.[7] We should notice that this value was calculated by assuming an absorption coefficient equal to one for the nanorods that overestimates the number of absorbed photons. Moreover, the device gain can also be further increased by applying a bias voltage larger than the value used in these experiments (400 mV). We ascribed the high calculated efficiency to (i) the use of small dimension active metal nanostructures that provided a more efficient generation of hot-carriers; (ii) electric field enhancement at the nanorod-nanowire interface that facilitated the electron injection and (iii) the low dimensionality of the semiconductor nanowire that provided an efficient path for charge collection.

A number of improvements could be proposed to further increase the presented device performances. For example, a reduction of the nanorod - nanowire distance by passivation of the nanorod surface would reduce the barrier at the interface and result in a more efficient hot-electron injection. Different semiconductor materials such as Si, GaN, GaAs, InP, InAs could in principle be used instead of ZnO to achieve a lower Schottky barrier, increasing carrier collection efficiency and also contributing directly to photocurrent generation by direct optical transition.

In conclusion, we investigated the enhanced photoconductance of hybrid Au nanorods-ZnO nanowire hybrid FET devices fabricated by a novel combined lithography/droplet deposition method. Compared to the bare ZnO nanowire FET, hybrid devices showed more than two orders

of magnitude enhanced photoconductivity and 40 times faster response for wavelengths in the range 650-850 nm. The improved performances were explained on the basis of plasmon-mediated hot-electron injection of photocarriers. The dependence of generated photocurrent from the metal nanostructure density and shape was investigated in details. The overall efficiency of ~3% was ascribed to a combined effect of the use of small dimension anisotropic active metal nanostructures and low dimensionality semiconductor nanowires.

The hybrid device presented in this work opens new avenues for the designing of novel miniaturized tunable photodetectors across the visible-near infrared region. Most importantly, the proposed architecture allows to highly engineering the optoelectronic properties of the single hybrid device by finely tuning the plasmonic resonances of Au nanorods and using homogeneous or heterostructured semiconductor nanowire with optimized optical and electrical properties. We believe that the miniaturized, tunable and integrated capabilities offered by metal nanorod-semiconductor nanowire device architectures presented in this work could have an important impact in many application fields such as opto-electronic sensors, photodetectors and photovoltaic devices.

ASSOCIATED CONTENT

Supporting Information. Details on synthesis and morphological analysis of Au nanorods and ZnO nanowire, photoconductivity measurements, electrical characterization and UV photoresponse of hybrid devices. This material is available free of charge via the Internet at http://pubs.acs.org

Acknowledgments. This work was supported by the European Commission under the Marie Curie project "Nanowiring" (265073), NMP project "Hysens" (263091), Science Foundation Ireland under the Research Frontiers Programme (SFI/09RFP/CAP2455) and the Irish Higher Education Authority PRTLI programs (Cycle 3 "Nanoscience" and Cycle 4 "INSPIRE") and the Irish Higher Education Authority Program for Research in Third Level Institutions (2007-2011) via the INSPIRE programme, by Science Foundation Ireland grant10/IN.1/I3000.

REFERENCES

1. Schuller, J. A.; Barnard, E. S.; Cai, W.; Jun, Y. C.; White, J. S.; Brongersma, M. L. *Nat. Mater.* **2010,** 9, (3), 193-204.
2. Endriz, J. G.; Spicer, W. E. *Phys. Rev. Lett.* **1970,** 24, (2), 64-68.
3. Zhao, G.; Kozuka, H.; Yoko, T. *Thin Solid Films* **1996,** 277, (1–2), 147-154.
4. Tian, Y.; Shi, X.; Lu, C.; Wang, X.; Wang, S. *Electrochem. Commun.* **2009,** 11, (8), 1603-1605.
5. Wu, F.; Hu, X.; Fan, J.; Liu, E.; Sun, T.; Kang, L.; Hou, W.; Zhu, C.; Liu, H. *Plasmonics* **2013,** 8, (2), 501-508.
6. Kochuveedu, S. T.; Kim, D.-P.; Kim, D. H. *J. Phys. Chem. C* **2011,** 116, (3), 2500-2506.
7. Knight, M. W.; Sobhani, H.; Nordlander, P.; Halas, N. J. *Science* **2011,** 332, (6030), 702-704.
8. Knight, M. W.; Wang, Y.; Urban, A. S.; Sobhani, A.; Zheng, B. Y.; Nordlander, P.; Halas, N. J. *Nano Lett.* **2013,** 13, (4), 1687-1692.
9. Fang, Z.; Liu, Z.; Wang, Y.; Ajayan, P. M.; Nordlander, P.; Halas, N. J. *Nano Lett.* **2012,** 12, (7), 3808-3813.
10. Soci, C.; Zhang, A.; Xiang, B.; Dayeh, S. A.; Aplin, D. P. R.; Park, J.; Bao, X. Y.; Lo, Y. H.; Wang, D. *Nano Lett.* **2007,** 7, (4), 1003-1009.
11. Yan, R.; Gargas, D.; Yang, P. *Nat Photon* **2009,** 3, (10), 569-576.
12. Hyun, J. K.; Lauhon, L. J. *Nano Lett.* **2011,** 11, (7), 2731-2734.
13. Chen, R.; Li, D.; Hu, H.; Zhao, Y.; Wang, Y.; Wong, N.; Wang, S.; Zhang, Y.; Hu, J.; Shen, Z.; Xiong, Q. *J. Phys. Chem. C* **2012,** 116, (7), 4416-4422.
14. Hu, M.-S.; Chen, H.-L.; Shen, C.-H.; Hong, L.-S.; Huang, B.-R.; Chen, K.-H.; Chen, L.-C. *Nat. Mater.* **2006,** 5, (2), 102-106.
15. Miao, J.; Hu, W.; Guo, N.; Lu, Z.; Zou, X.; Liao, L.; Shi, S.; Chen, P.; Fan, Z.; Ho, J. C.; Li, T. X.; Chen, X. S.; Lu, W. *ACS Nano* **2014,** 8, (4), 3628-35.
16. Casadei, A.; Pecora, E. F.; Trevino, J.; Forestiere, C.; Ruffer, D.; Russo-Averchi, E.; Matteini, F.; Tutuncuoglu, G.; Heiss, M.; Fontcuberta i Morral, A.; Dal Negro, L. *Nano Lett.* **2014,** 14, (5), 2271-8.
17. Chu, S.; Wang, G.; Zhou, W.; Lin, Y.; Chernyak, L.; Zhao, J.; Kong, J.; Li, L.; Ren, J.; Liu, J. *Nat Nano* **2011,** 6, (8), 506-510.

18. Gimenez, A. J.; Yáñez-Limón, J. M.; Seminario, J. M. *J. Phys. Chem. C* **2010,** 115, (1), 282-287.
19. Wang, Z. L. *J. Phys.: Condens. Matter 16 (2004) R829–R858* **2004**.
20. Zhang, H.; Babichev, A. V.; Jacopin, G.; Lavenus, P.; Julien, F. H.; Egorov, A. Y.; Zhang, J.; Pauporte, T.; Tchernycheva, M. *J. Appl. Phys.* **2013,** 114, (23), 234505.
21. Fang, Y. J.; Sha, J.; Wang, Z. L.; Wan, Y. T.; Xia, W. W.; Wang, Y. W. *Appl. Phys. Lett.* **2011,** 98, (3), 033103.
22. Cheng, C. W.; Sie, E. J.; Liu, B.; Huan, C. H. A.; Sum, T. C.; Sun, H. D.; Fan, H. J. *Appl. Phys. Lett.* **2010,** 96, (7), 071107-3.
23. Dhara, S.; Giri, P. K. *J. Appl. Phys.* **2011,** 110, (12), 124317-9.
24. Bera, A.; Basak, D. *Appl. Phys. Lett.* **2009,** 94, (16), 163119.
25. Moazzami, K.; Murphy, T.; Phillips, J.; Cheung, M. C.; Cartwright, A. *Semicond. Sci. Technol.* **2006,** 21, (6), 717.
26. Liao, Z.-M.; Zhang, H.-Z.; Zhou, Y.-B.; Xu, J.; Zhang, J.-M.; Yu, D.-P. *Phys. Lett. A* **2008,** 372, (24), 4505-4509.
27. Dhara, S.; Giri, P. *Nanoscale Research Letters* **2011,** 6, (1), 504.
28. Studenikin, S. A.; Cocivera, M. *J. Appl. Phys.* **2002,** 91, (8), 5060-5065.
29. Lany, S.; Zunger, A. *Phys. Rev. B* **2005,** 72, (3), 035215.
30. Liu, K. W.; Chen, R.; Xing, G. Z.; Wu, T.; Sun, H. D. *Appl. Phys. Lett.* **2010,** 96, (2), 023111.
31. Zhang, A.; You, S.; Soci, C.; Liu, Y.; Wang, D.; Lo, Y.-H. *Appl. Phys. Lett.* **2008,** 93, (12), 121110.
32. González-Posada, F.; Songmuang, R.; Den Hertog, M.; Monroy, E. *Nano Lett.* **2011,** 12, (1), 172-176.
33. Clavero, C. *Nat Photon* **2014,** 8, (2), 95-103.
34. Boettcher, S. W.; Strandwitz, N. C.; Schierhorn, M.; Lock, N.; Lonergan, M. C.; Stucky, G. D. *Nat. Mater.* **2007,** 6, (8), 592-596.
35. Aradhya, S. V.; Frei, M.; Hybertsen, M. S.; Venkataraman, L. *Nat. Mater.* **2012,** 11, (10), 872-876.
36. Pescaglini, A.; O'Riordan, A.; Quinn, A. J.; Iacopino, D. *J. Mater. Chem. C* **2014**.
37. Bernard, L.; Kamdzhilov, Y.; Calame, M.; van der Molen, S. J.; Liao, J.; Schönenberger, C. *J. Phys. Chem. C* **2007,** 111, (50), 18445-18450.
38. Liao, J.; Bernard, L.; Langer, M.; Schönenberger, C.; Calame, M. *Adv. Mater.* **2006,** 18, (18), 2444-2447.
39. Li, Q. H.; Gao, T.; Wang, Y. G.; Wang, T. H. *Appl. Phys. Lett.* **2005,** 86, (12), 123117.
40. Fowler, R. H. *Physical Review* **1931,** 38, (1), 45.
41. Lin, Y.-J.; Tsai, C.-L. *J. Appl. Phys.* **2006,** 100, (11), 113721.
42. Govorov, A. O.; Zhang, H.; Demir, H. V.; Gun'ko, Y. K. *Nano Today* **2014,** 9, (1), 85-101.
43. Govorov, A. O.; Zhang, H.; Gun'ko, Y. K. *J. Phys. Chem. C* **2013,** 117, (32), 16616-16631.
44. Zhang, H.; Govorov, A. O. *J. Phys. Chem. C* **2014,** 118, (14), 7606-7614.
45. Jones, T. B., *Electromechanics of particles*. Cambridge Univ Pr: 2005.
46. Liu, N.; Mukherjee, S.; Bao, K.; Brown, L. V.; Dorfmuller, J.; Nordlander, P.; Halas, N. J. *Nano Lett.* **2012,** 12, (1), 364-9.

47. Manjavacas, A.; Liu, J. G.; Kulkarni, V.; Nordlander, P. *ACS Nano* **2014,** 8, (8), 7630-7638.